A Comprehensive Mechanistic Scenario for the Cu-Mediated Asymmetric Propargylic Sulfonylation forging Tertiary Carbon Stereocenters

Aleria Garcia-Roca,[§,¥,‡] Raúl Pérez-Soto,[§,¥,‡] Georgiana Stoica,[§] Jordi Benet-Buchholz,[§] Feliu Maseras[§,*] and Arjan W. Kleij[§,†*]

[§] Institute of Chemical Research of Catalonia (ICIQ), the Barcelona Institute of Science and Technology (BIST), Av. Països Catalans 16, 43007 Tarragona (Spain). E-mail: fmaseras@iciq.es, akleij@iciq.es

[¥] Departament de Química Física i Inorgánica, Universitat Rovira i Virgili, Marcel·lí Domingo s/n, 43007 Tarragona (Spain)

[†] Catalan Institute of Research and Advanced Studies (ICREA), Pg. Lluïs Companys 23, 08010 Barcelona (Spain)

[‡] A.G.R. and R.P.S. contributed equally to this work.

ABSTRACT: Metal-catalyzed propargylic transformations represents a powerful tool in organic synthesis to achieve new carbon-carbon and carbon-heteroatom bonds. However, detailed knowledge about the mechanistic intricacies related to the asymmetric formation of propargylic products featuring challenging heteroatom-substituted tertiary stereocenters is scarce, and therefore provides an inspiring challenge. Here, we present a meticulous mechanistic analysis of a propargylic sulfonylation reaction promoted by a chiral Cu catalyst through a combination of experimental techniques and computational studies. Surprisingly, the enantio-discriminating step is not the coupling between the nucleophile and the propargylic precursor but rather the following proto-demetalation step, a scenario further validated by computing enantio-induction levels under other previously reported experimental conditions. A full mechanistic scenario for this propargylic substitution reaction is provided including a catalyst pre-activation stage, a productive catalytic cycle and an unanticipated non-linear effect at the Cu(I) oxidation level.

INTRODUCTION

Asymmetric metal-catalyzed propargylic substitution reactions display high utility in synthetic chemistry allowing to quickly diversify and functionalize a wide range of suitable achiral precursors with a broad range of nucleophiles.[1] These transformations are useful toward the construction of new stereogenic centers, which are conventionally forged in the presence of transition metal catalysts derived from ruthenium, rhodium and palladium. However, in the last two decades, catalysts based on more abundant metals such as copper and nickel have emerged as powerful alternatives thereby significantly expanding the chemical space that can be accessed through propargylic activation patterns.[2] During the 2000´s, both Nishibayashi[3] and van Maarseveen[4] independently reported on copper-catalyzed enantioselective propargylic amination reactions employing bidentate phosphorus- and nitrogen-based ligands, respectively (Scheme 1a). Ever since these seminal examples, copper catalysts have been frequently used in asymmetric propargylic substitution reactions exploring an increasingly diverse set of (pro)nucleophiles[1a-b,2,5,6] and providing in most cases products featuring a secondary carbon stereocenter.

We have become interested in the catalytic asymmetric formation of sterically congested carbon stereocenters[7] as these are frequently encountered in many biologically active molecules and pharmaceutical precursors.[8] In 2019, we reported the enantioselective propargylic sulfonation of alkyne-substituted cyclic carbonates to afford compounds with tertiary carbon stereocenters (Scheme 1b), with a clear non-linear effect (NLE) observed between the enantioselectivity of the transformation and the enantio-purity of the chiral Cu catalyst.[9] While mechanistic analysis of catalytic propargylic substitution processes leading to either tetrasubstituted tertiary or quaternary carbon stereocenters remains rare,[6a,d] Nishibayashi and coworkers reported that Cu(PyBox) complexes form dinuclear species that account for the observed NLE in their propargylation protocol.[6a] The intermediacy of a $Cu_2(Pybox)_2$ complex was also suggested by the same authors in separate studies for the formation of secondary carbon stereocenters,[5b,d] and more recently by Niu.[5a] The enantio-induction was explained by catalyst control during the attack of the nucleophile onto an intermediate Cu(allenylidene) species (Scheme 1c).[10a]

With these typical characteristics in mind, we wondered whether our propargylic sulfonylation propelled by Cu-catalysis[9] and displaying a clear NLE would follow a similar pathway involving dinuclear metal intermediates. Furthermore, in our original work a clear influence of the nature

of the propargylic precursor on the level of enantio-discrimination was noted, which prompted us to find a rationale for this peculiar observation. Here, we report on a detailed experimental and computational analysis of this propargylic substitution reaction.

Scheme 1. (a) Seminal Examples of Cu-Mediated Propargylic Substitution, (b) Previous Cu-Promoted Propargylic Sulfonylation, and (c) Established Mechanistic Picture versus New Insights (This Work)

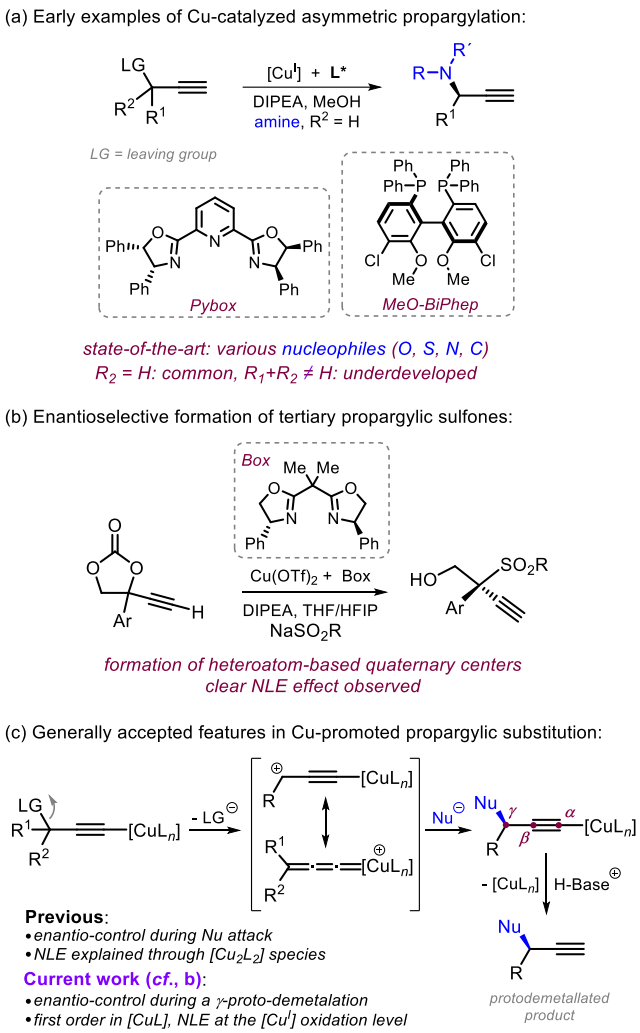

The combined data reveal that this coupling manifold is promoted by a *mono*-nuclear Cu^{I}Box (Box = bisoxazoline) complex, and the previously observed NLE is explained by a significant difference in stability between *homo*- and *hetero*-chiral Cu^{I}(Box)$_2$ complexes, which is clearly distinct from recently described NLE effects with similar complexes at the Cu(II) oxidation level.[11] A theoretical model was developed and validated against experimental findings revealing an unexpected rationalization of the enantio-induction. The latter occurs beyond the coupling step that involves the sulfonate nucleophile, being a formal γ-protodemetalation of the Cu complex from the eventual product.[12] The collected information (Scheme 1c) thus provides a rather different mechanistic scenario compared to the state of the art, and highlights a delicate structural balance that may exist in the catalytic formation of sterically demanding carbon stereocenters.

RESULTS AND DISCUSSION

Order in [Cu] and Oxidation State of Active Species. One of the aspects to address is the understanding of how the copper precursor is promoted towards an active chiral catalyst. We first performed kinetic studies to determine the order in the Cu-complex derived from Cu(OTf)$_2$ and the chiral Box ligand (**L*RR***) previously used in this propargylic sulfonylation reaction (Figure 1a).[9] We took advantage of the carbonate functional group present in the propargylic surrogate **A**, whose fingerprint absorption is easily followed by React-IR (Figure 1b). The kinetic data that was obtained was analyzed by variable time normalization analysis (VTNA),[13] which provided a first order dependency in Cu catalyst. This led us to consider a monometallic copper complex as the active species in the rate-limiting step of the process. The React-IR analysis also allowed to detect and monitor the CO_2 band (cf., decarboxylation of the substrate **A**), providing evidence for the gradual formation of the target sulfone product **B** (Figure 1, and the Supporting Information, SI).

Next, we examined the reaction described in Figure 1a by Electron Paramagnetic Resonance (EPR) and followed the catalytic process in time (Figure 1c) facilitated by the characteristic bands of the Cu(II)Box complex. A significant decrease of the Cu(II) signal during the first 30 minutes of the reaction was observed that did not change much after 24 h. These results suggest that the Cu(II) species is reduced to an EPR-silent Cu(I) complex, which likely enters the productive catalytic cycle. Intrigued by this observation, we wondered which reaction component(s) is/are responsible for the apparent reduction of the metal species and conducted several control experiments (Figure 1d) by a step-wise addition protocol using the same relative amounts used under optimized conditions.[9]

The complexation between the copper salt and the chiral ligand **L*RR*** displayed the expected formation of a Cu(II) complex (turquoise color in solution) with a characteristic EPR pattern different from the one observed in Figure 1c after 2 min. However, upon addition of DIPEA, a dark blue solution was formed with a distinctive EPR trace partially matching the EPR spectrum at 2 min of the reaction mixture (Figure 1d), suggesting that the base plays an imperative role to advance the coupling process. Following base addition, the next component supplied to the EPR probe solution was the alkyne-substituted cyclic carbonate **A**. At this stage, we observed a slight shift of the EPR band and a concomitant color change of the mixture to red. The change in the EPR behavior of the Cu complex is indicative for a change in its coordination environment. Finally, upon addition of the nucleophile ($NaSO_2Ph$), the EPR signal becomes silent which is consistent with the

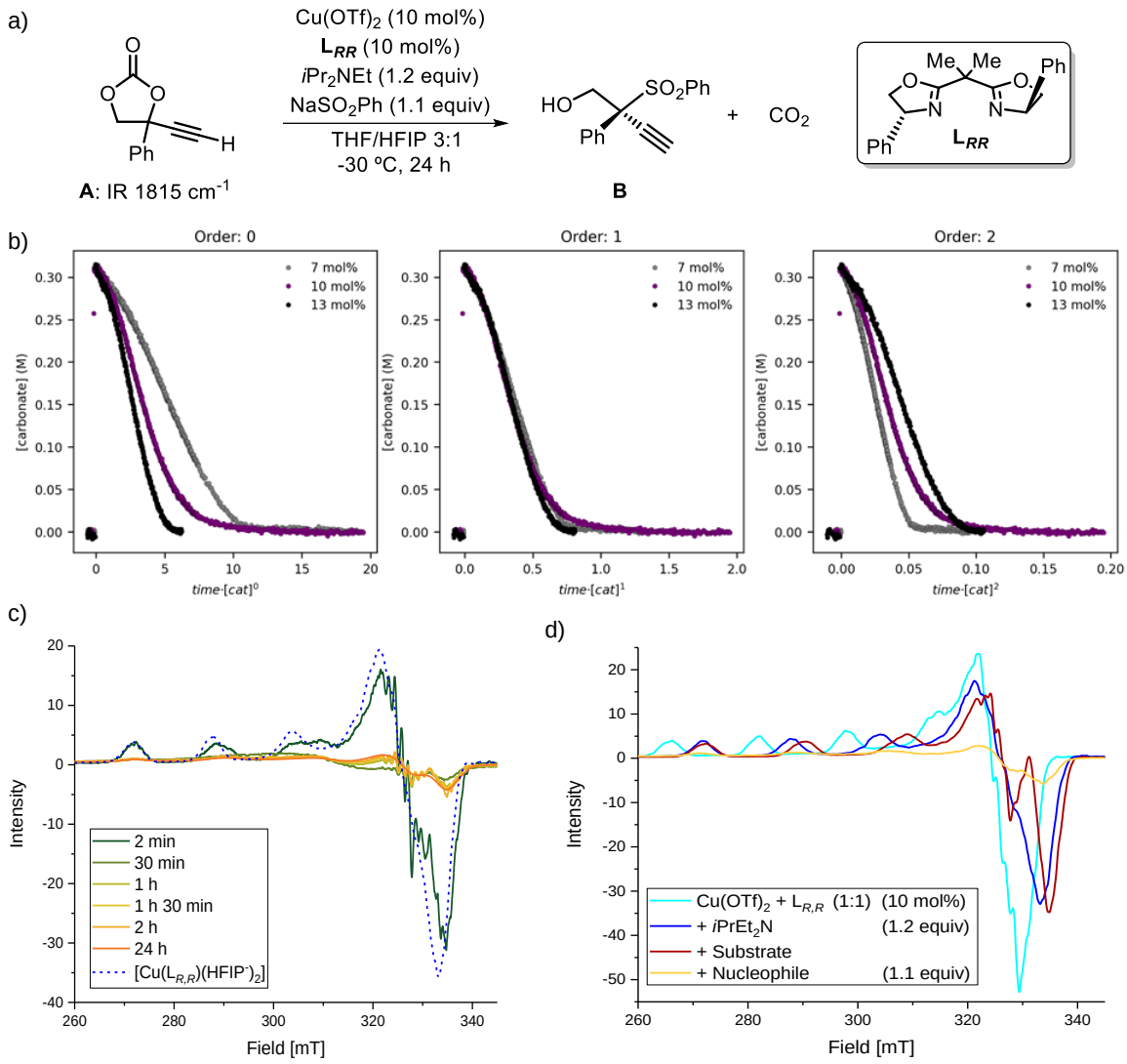

Figure 1. a) Benchmark reaction, b) Order of catalyst by VTNA analysis plots and c) EPR monitoring of the catalysis (left) and EPR analysis of catalyst evolution upon addition of reagents (right).

previous observation under the standard catalytic conditions (Figure 1c). The experimental findings suggest that both the substrate (with time) as well as the sulfonate salt are capable reductants, with the latter being more potent. These trends could be qualitatively reproduced by B3LYP-D3 based DFT calculations (SI) with the investigated semi-reduction and –oxidation reactions further promoted in the presence of hexafluoro-*iso*-propanol (HFIP, the co-solvent used). The gradual changes in the EPR spectrum after sequential addition of the different reaction components suggest that different intermediate species are formed during the catalytic process, and thus their isolation and identification would shed further light on the catalyst pre-activation pathway.

Identification of Intermediate Cu-Complexes. We initially examined the complexation between a 1:1 stoichiometric ratio of $Cu(OTf)_2$ and the chiral ligand $\mathbf{L_{RR}}$ in THF/HFIP (3:1 v/v), and the turquoise product **1** was crystallized (62% of crystalline material) and characterized by X-ray crystallography (Scheme 2a). The molecular structure of **1** (Scheme 2b) reveals an octahedral Cu-complex with two water molecules coordinated in the equatorial positions.[14] The presence of coordinating water molecules is in line with the experimental conditions that do not need to be strictly anhydrous for productive catalysis. To support this view, we also carried out the same complexation reaction between $Cu(OTf)_2$ and $\mathbf{L_{RR}}$ under dry conditions. Under anhydrous conditions, a different green-colored Cu(II) complex is formed and X-ray analysis revealed the main product to be a Cu-complex (**2**, Scheme 2b) with a 2:1 ligand-to-metal ratio. Complex **2** could be independently prepared by treatment of $Cu(OTf)_2$ with 2 equiv of $\mathbf{L_{RR}}$ providing the same product with a 95% yield (powder; 72% yield of crystalline material).[15]

Scheme 2. Synthesis and Characterization of Cu(II) and Cu(I) complexes 1-5 (a), and X-ray Analysis of Complexes 1-5 (Anions not shown) with Displacement Ellipsoids at the 50% Probability Level

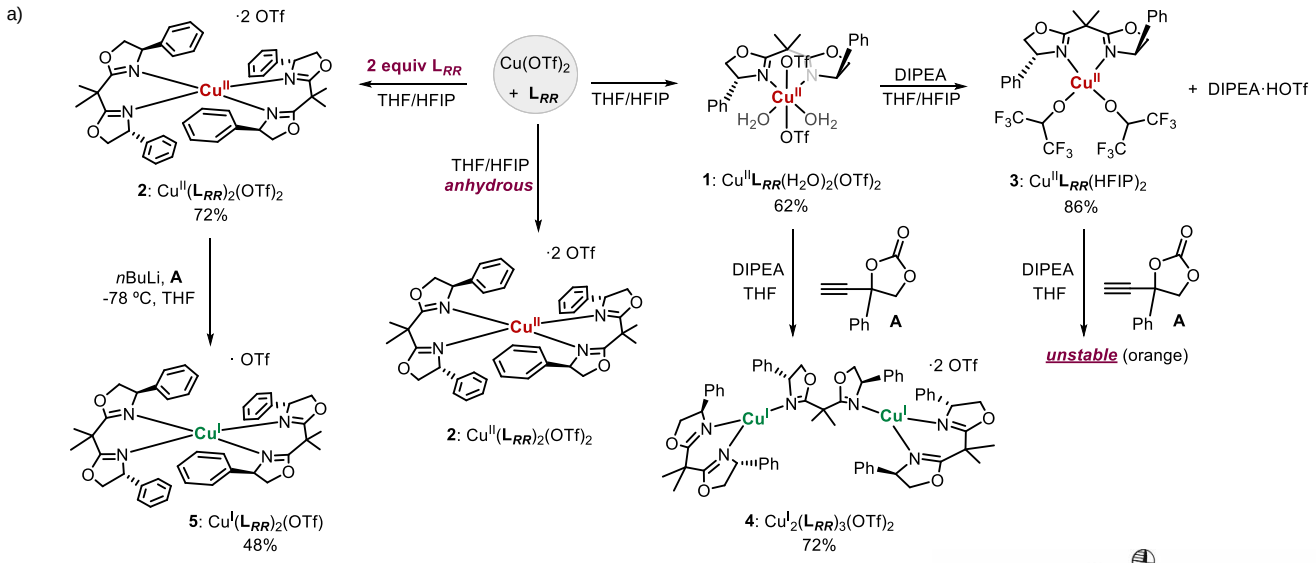

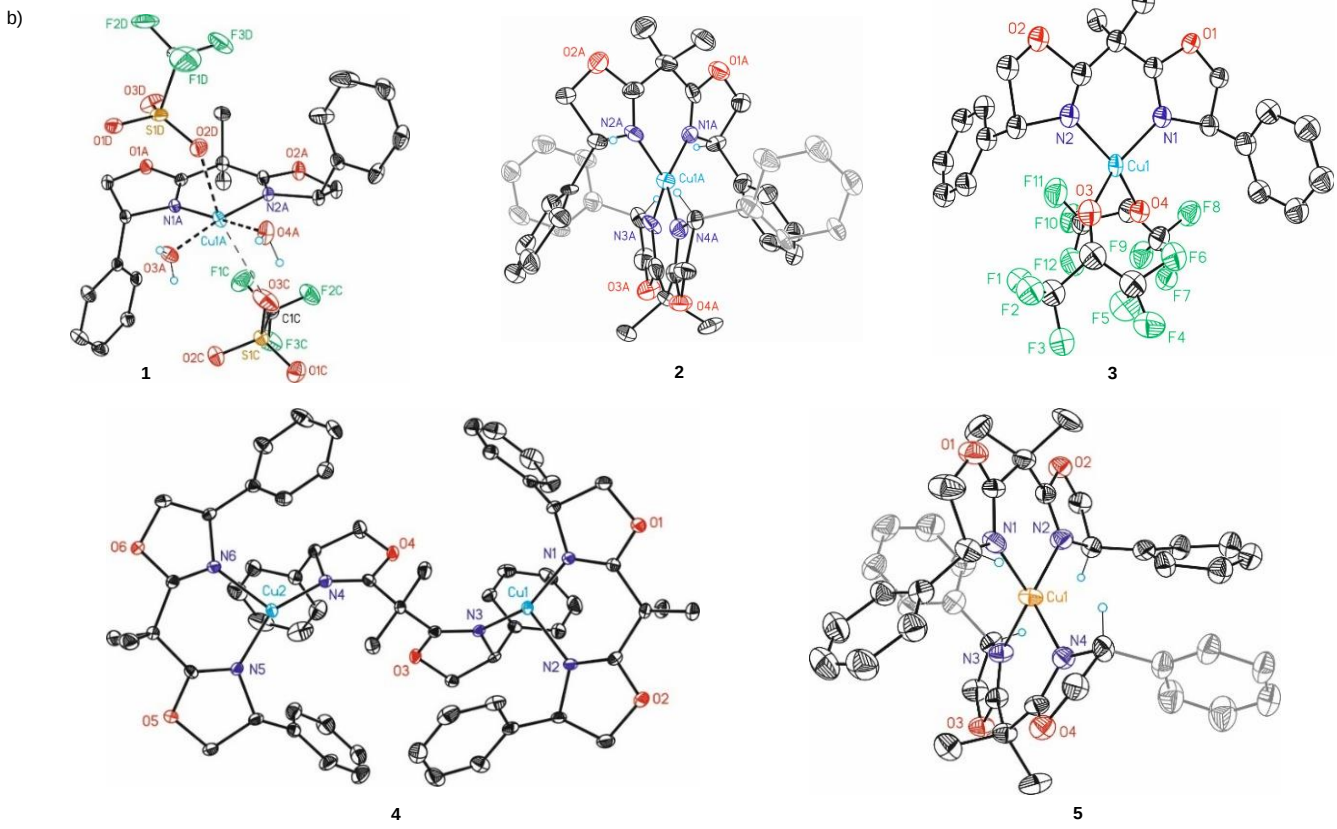

Since the sulfonylation process is carried out under basic conditions (DIPEA) and using HFIP as a co-solvent, we evaluated the role of both components. When DIPEA was added into a THF/HFIP solution of **1**, a new dark blue Cu(II) complex (**3**, 86% of crystalline material) could be isolated. X-ray analysis of **3** (Scheme 2b) showed this Cu-complex to be a distorted square-planar complex with two deprotonated molecules of HFIP coordinating to the metal center. The difference in the EPR spectra of both **1** and **3** can thus be explained by a geometrical change from octahedral to square planar (see also the SI). From the same reaction, the salt DIPEA·HOTf was crystallographically identified as an expected by-product (SI).

With two of the intermediate Cu(II) complexes being structurally characterized, we then attempted to identify the complex related to the third stage of the sequential EPR study reported in Figure 1d (i.e., the red trace). Complex **2** was mixed with 1.5 equiv of substrate **A** and 2.5 equiv of DIPEA in a 3:1 THF/HFIP solvent mixture. Unfortunately,

Scheme 3. Reported NLE effect in Propargylic Sulfonylation of Substrate A with $NaSO_2Ph$ giving Sulfone Product B (a), Cationic part of the X-ray Structure for Heterochiral Cu(II) Complex 6 (b), and Relative Free Energies in kcal/mol Computed for the Cationic Part of the Homo- and Heterochiral $Cu(II)L_2$, $Cu(I)L_2$ and $Cu(I)L_3$ Complexes 2, 4 and 5 (c)

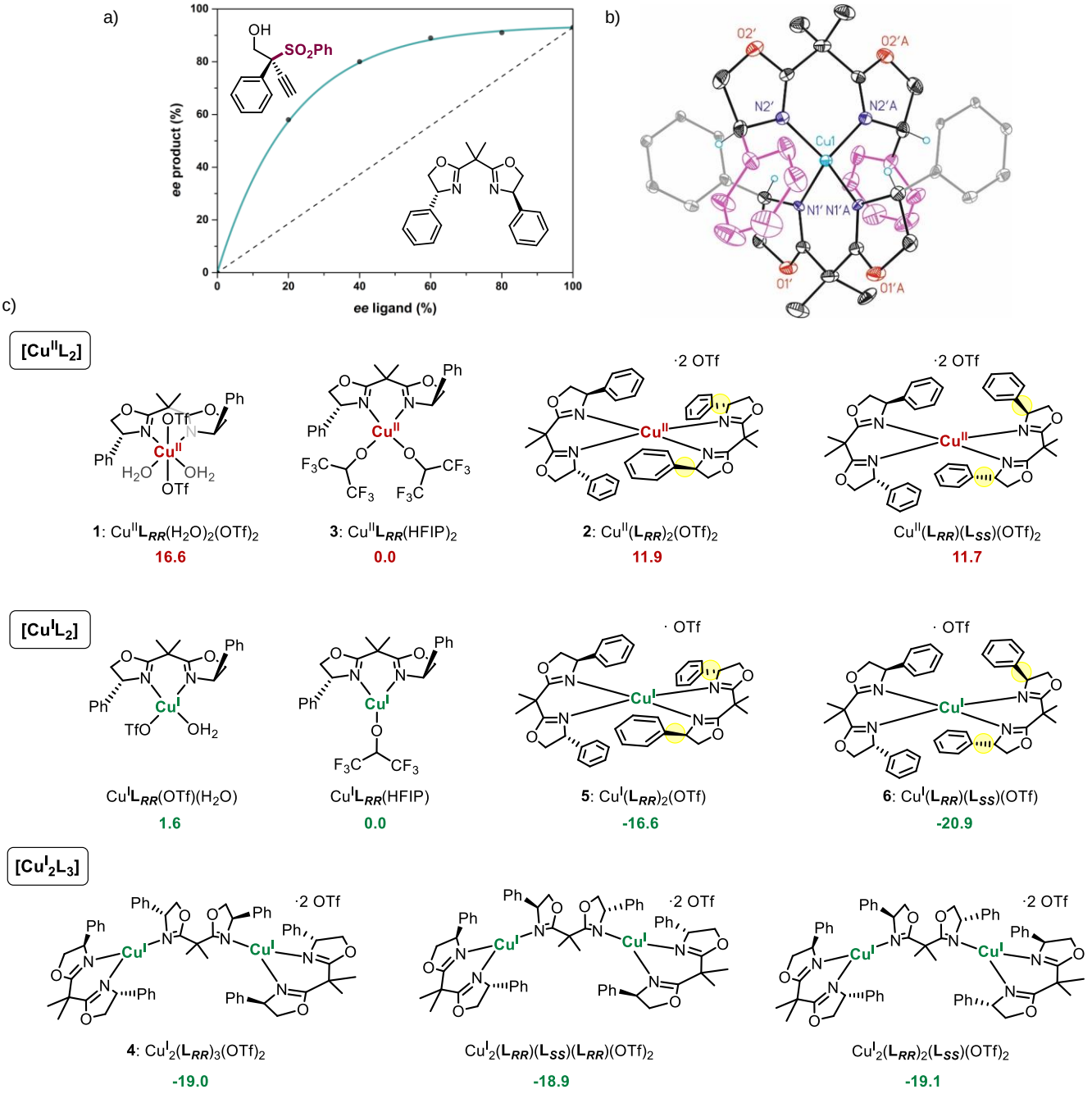

we could not isolate nor further characterize this last Cu(II) intermediate due to its instable character. To understand the observed *in situ* reduction of Cu(II) in the reaction medium, efforts were made to isolate the assumed Cu(I) complex by reacting complex **1** with substrate **A** in the presence of DIPEA (Scheme 2a). Fortunately, a yellow-colored complex (**4**) could be isolated in crystalline form (72%), and its crystallographic analysis (Scheme 2b) demonstrated an unexpected stoichiometry $[Cu_2(\mathbf{L}_{RR})_3{\cdot}2OTf]$ with one Box ligand bridging between two Cu(I)Box complexes having an unusual and rare T-shaped coordination geometry.[16] Interestingly, when the green Cu(II) complex **2** was treated with a deprotonated version of alkynyl carbonate **A** under inert conditions, a structurally related Cu(I) complex (**5**, 43%, Scheme 2a+b) was isolated as a pale-brown crystalline solid.[17] The formation of both Cu(I) complexes **4** and **5** are in line with the reductive potential of the catalytic reaction mixture, and together with the EPR studies (Figure 1d) and the first-

order dependence on Cu$\mathbf{L}_{RR}$ suggest that a mono-nuclear Cu(I) species enters the productive cycle.

Complexes **4** and **5** were used as potential pre-catalysts for the propargylic sulfonylation reaction with **A** and $NaSO_2Ph$ as substrates under the optimized reaction conditions (Figure 1a; SI for details).[9] While the presence of complex **4** did not lead to any observable conversion of substrate, complex **5** showed catalytic potential with a 30% yield noted for propargylic sulfone **B** and with a comparable level of enantio-induction (97:3 *er*) as determined previously (96.5:3.5 *er*).[9] Whereas complex **4** should be merely regarded as a structural model, **5** can be regarded as a realistic, functional model and further sustains the proposal of an active Cu(I) species as catalyst. This aligns well with the EPR observations that show a gradual decrease of the Cu(II) species (Figure 1c+d) under the catalytic conditions, and further corroborates with our previous experimental findings that the presence of either a Cu(II) or Cu(I) precursor barely influences the product yield or the level of asymmetric induction.[9]

Non-Linear Effect (NLE). Previously we observed a clear positive NLE for the sulfonylation reaction of substrate **A** (Figure 1a and Scheme 3a). In order to explain this behavior, we considered the possibility of *in situ* formation of [CuL_2] species following the model introduced by Kagan.[18] Relevant to our system are the detailed studies performed by Franz and co-workers, who previously determined the origin of the NLE in a Cu(Box) catalyzed asymmetric spiro-annulation reaction.[11] In these latter studies, EPR spectroscopy was used to support the formation of an inactive CuL_2 type species (*based on the same Ph-Box ligand* ***L*** *used in our studies*) in the presence of scalemic ligand mixtures, with heterochiral CuL_2 being more stable than the homochiral one thus causing a positive NLE.

We therefore first assessed the relative stability of the homo- (*i.e.*, **2**) and hetero-Cu$\mathbf{L}_2$ complexes. With homo-complex Cu($\mathbf{L}_{RR}$)$_2$ **2** already available (Scheme 2a), first an attempt was made to prepare the heterochiral complex Cu($\mathbf{L}_{RR}\mathbf{L}_{SS}$) from a 1:1:1 stoichiometric combination of $Cu(OTf)_2$, $\mathbf{L}_{RR}$ and $\mathbf{L}_{SS}$. The green product (*rac*-**6**, 64% of crystalline product; see SI for details) was examined by X-ray diffraction, and after careful refinement the measured crystal was shown to be a mixture of Cu($\mathbf{L}_{RR}$)$_2$ (42.5 %), Cu($\mathbf{L}_{SS}$)$_2$ (42.5 %) and Cu($\mathbf{L}_{RR}\mathbf{L}_{SS}$) (15 %). The structural differences between the homo- (complex **2**) and heterochiral complex (present in crystalline **6,** Scheme 3b) could be scrutinized, and both structures appeared to be rather similar. To further evaluate the relative stabilities, several other experiments were carried out. Both pre-isolated homo- and *rac*-CuL_2 complexes **2** and **6** are converted into their respective $CuL(HFIP)_2$ derivatives in the presence of DIPEA in TFH/HFIP (3:1) as evidenced by EPR (SI). Furthermore, when homochiral **2** is EPR-titrated with $\mathbf{L}_{SS}$, a clear dynamic ligand behavior is observed pointing at the formation of a mixture of both homo- and heterochiral Cu$\mathbf{L}_2$ reminiscent of the mixture found in crystalline **6** (see the SI).

The preferred speciation of Cu(II) complex **2** was then studied by DFT (see the SI for details) using the X-ray data of **1**, **2** and **3** as input, and the relative free energies of the homo- and heterochiral complex compared to those associated with aquo-complex **1** and HFIP complex **3** (Scheme 3c). While both homo/hetero Cu$\mathbf{L}_2$ complexes have fairly similar energies (11.9 vs 11.7 kcal/mol, respectively), the HFIP complex **3** is significantly more stable (0.0 kcal/mol, used as reference state), which is in line with the experimental observation of easy ligand dissociation from **2** in the presence of HFIP. The aquo-complex **1** has a slightly higher free energy (16.6 kcal/mol) than homo/heterochiral **2**, and dissociation of the latter in the presence of (excess) water could evolve into a mixture, which was indeed experimentally observed by EPR titrations (see the SI).

The combined spectroscopic and computational data collected for the Cu(II) complexes of type Cu$\mathbf{L}_2$ cannot explain the positive NLE that is noted in this propargylic sulfonylation process. Since stable Cu(I) complexes **4** and **5** could be identified, we then turned our focus on the possibility that these species could function as relatively inactive, off-cycle compounds and be responsible for the non-linear relationship between the enantio-purity of the Cu catalyst and the *ee* of the product **B**. The relative free energies of both kinds of Cu(I) derivatives were investigated by DFT (Scheme 3c and SI), and notably a different trend was observed within this series. Both homo- and heterodimers of Cu(I) complex **5** are significant more stable (-16.6 and −20.9 kcal/mol, respectively) than Cu(I)**L**(HFIP) or Cu(I)**L**(H_2O)(OTf) at 0.0 and 1.6 kcal/mol, respectively. Similarly, for the bis-Cu(I) complex **4** with a T-shaped coordination environment, the homo- and heterochiral derivatives were also much more stable than the HFIP-coordinated Cu(I) complex (Scheme 3c, energies around 19 kcal/mol). These theoretical results match well with the experimental notion that the addition of a large excess of HFIP to either **4** or **5** in the presence of DIPEA did not alter their UV-vis spectra (see SI). In addition, the above calculations combined with the observed NLE, the activity of mononuclear **5** and inactivity noted for dinuclear **4** in the coupling of carbonate substrate **A** and sodium sulfinate suggest that a mononuclear Cu(I) complex is the dominant active species.

At the Cu(I) oxidation level (i.e., for **5**), the heterochiral complex is more stable than the homochiral one by 4.3 kcal/mol, which rationalizes the origin of the observed NLE with the Cu(I)$\mathbf{L}_{RR}\mathbf{L}_{SS}$ likely not participating as a pre-catalyst in the asymmetric coupling reaction. Although only a slight excess of ligand (10%) is used under the optimized reaction conditions, we also examined homo- and heterochiral $Cu_2\mathbf{L}_3$ type complexes of **4** as potential reservoirs, but we found that their computed energies are quite similar (Scheme 3c, bottom) within a range of 0.2 kcal/mol. Therefore, the NLE cannot be justified by these data, and is best explained by the formation of inactive Cu(I)$\mathbf{L}_{RR}\mathbf{L}_{SS}$.

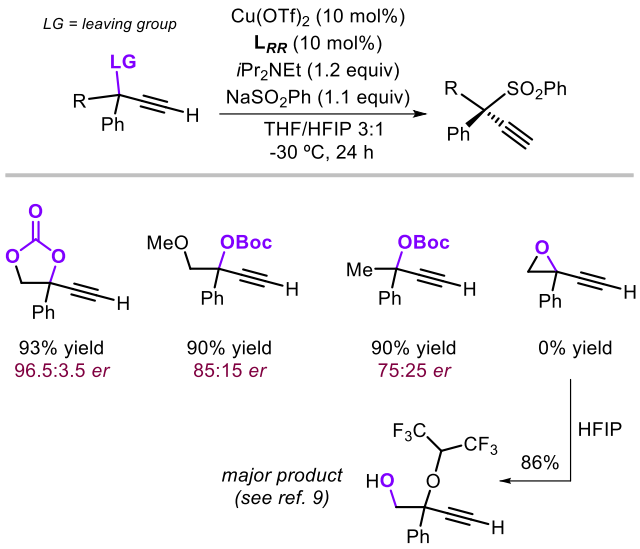

Figure 2. Effect of the propargylic precursor on the reaction efficiency.

Productive Catalytic Cycle. With the identification of the key species involved, the order in Cu complex established, and the NLE accounted for, a thorough computational analysis of the catalytic formation of propargylic sulfone **B** from substrate **A** and $NaSO_2Ph$ was conducted to elucidate the origin of the chiral induction, and the role of the propargylic precursor as previously we found that the structural identity of the substrate plays an imperative role (Figure 2) on the reactivity and enantio-induction,[19] with lower enantiocontrol noted for other propargylic precursors and a completely distinct reactivity for alkynyl epoxides.[9]

Inspired by the work of Nishibayashi, we calculated the catalytic cycle (Figure 3 and SI) following the generally accepted overall steps.[1b,10d] After initial coordination of **A** to the Cu(I) catalyst (**Io**) also the nucleophile may interact (reversibly) with **Io** leading to the initial resting state of the system (**IoNu**). Then, the first step onwards is a deprotometalation of substrate **A** assisted by the base (DIPEA) leading to Cu-acetylide intermediate **I3**. **I3** could in principle be directly attacked by the sulfinate, but we discarded this option because of the high barrier associated to an S_N2 attack on a quaternary carbon. Such a mechanism might, however, play a role when epoxides are used as starting material leading to different products. The reaction in Figure 3 continues through the generation of a carbocation (**I8**) that in the case of **A** comprises two consecutive steps. The first is a ring opening of the cyclic carbonate leading to intermediate **I4**. We could not locate the transition state for this ring-opening, but the barrier is likely low as a result of a scan performed (details reported in the SI). The process consists mostly of the rotation of the carbonate fragment away from the tertiary carbon center, a movement which essentially involves rotation around a single bond. This ring opening is followed by a decarboxylation step assisted by a proton transfer from the protonated base (**I5**→**I7** via **TS2**) leading to **I8**. Obviously, intermediate **I5** can be also depicted as a formal Cu-allenylidene species providing as such resonance stabilization.[5c,10a,c] After the formation of the adducts **I9r** and **I9s** (which can be interconverted without the need for full dissociation), the third key step of the mechanism corresponds to C–S bond formation through a nucleophilic attack of the SO_2Ph anion (**I9**→**I10** via **TS3**) on the carbocation in γ-position. The final step is a proto-demetalation of the product assisted by a protonated base molecule (**I12**→**I13** via **TS4**) followed by the release of the base and the propargylic sulfone product and the coordination of a new molecule of the substrate (**I13**→**I14**→**Io'**) to induce subsequent turnover.

The energetic span of this manifold (18.0 kcal/mol) is compatible with a reaction that occurs slowly at –30 ºC providing nonetheless a high yield of enantio-enriched product **B** after 24 h. The highest point in the depicted free energy profile corresponds to a zwitterionic product (**I4**) after ring opening of the cyclic carbonate with the following transition states and intermediates being downhill in energy. Thus, from these calculations we conclude that the deproto-metalation step and the carbonate ring opening are part of the rate determining trajectory of the process (i.e., **Io** to **I4** in Figure 3).

Origin of the Enantioselectivity. Generally, the formation of a stereogenic center during a propargylic substitution process is considered to occur during the nucleophilic attack on a metal-acetylide or metal-allenylidene species. Therefore, we initially believed that the enantioselection takes place during C–S bond formation (**I9**→**I10** via **TS3**). DFT modeling of this step is challenging and we were unable to find a transition state structure due to the bimolecular and highly exergonic nature of this step when considering the nucleophilic sulfinate alone (SI). We initially addressed this issue by performing relaxed scans of the C–S bond dissociation (SI). The two lowest conformations per each diastereomer with their respective dissociations were calculated showing a potential energy profile similar to that of a barrierless process. Fortunately, when we considered the formation of an adduct between **I8** and an ion pair of the sulfinate anion and a protonated DIPEA, we were able to find transition states **TS3r** and **TS3s**.These transition states showed small imaginary frequencies that, coupled with the non-covalent nature of intermediates **I9s** and **I9r** lead to difficult to converge conformations. As a consequence, we can only state that those transition states provide an estimate of the upper limit of the barriers of the nucleophilic attack.

According to the current results a kinetic competition should happen between transition states **TS4r** and **TS4s**, which would lead to the observed (*S*)-configured sulfone. The proto-demetalation thus plays a key role to control the enantiomeric ratio of the product. These computational

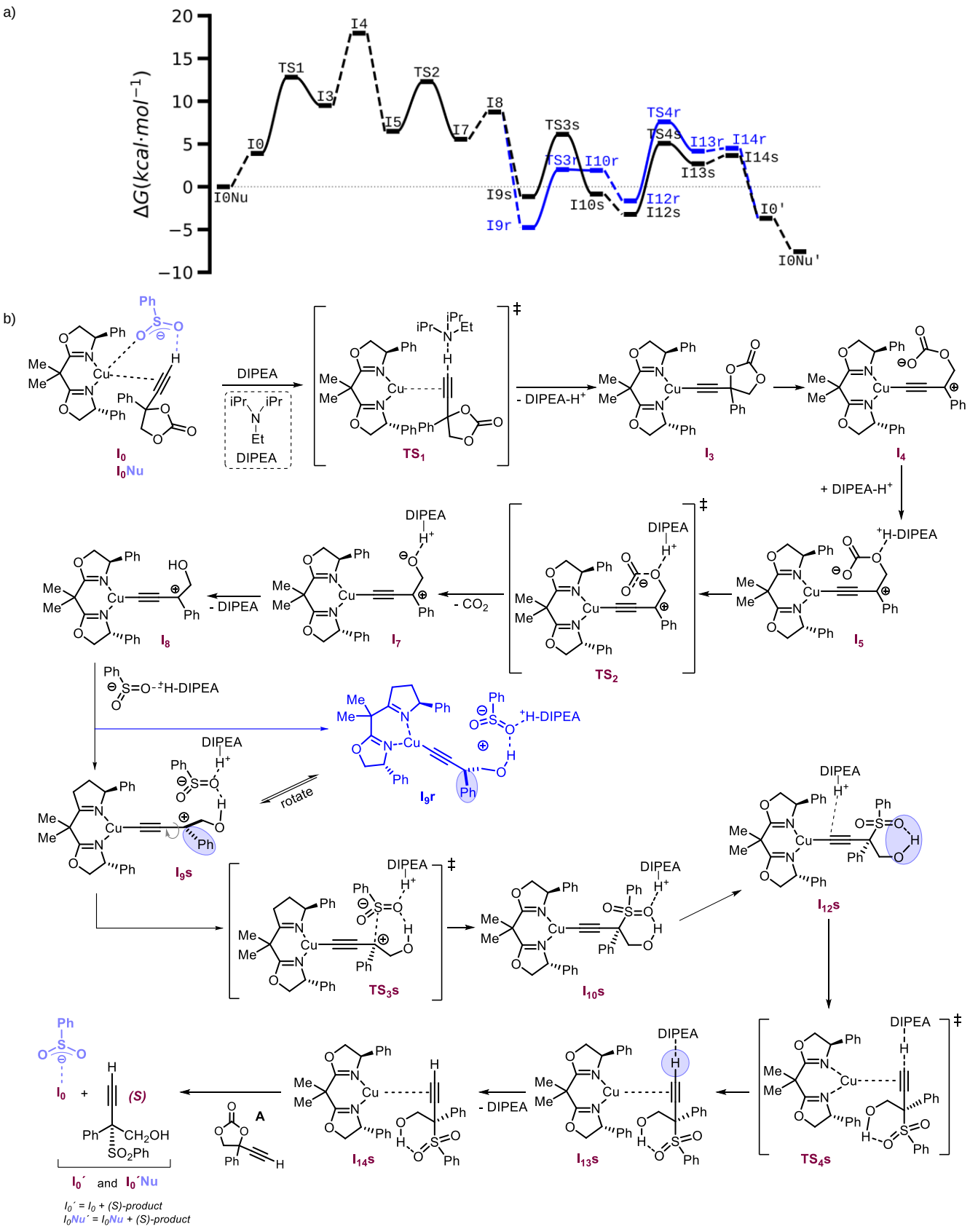

Figure 3. (a) Gibbs free energy profile and (b) mechanistic proposal for the Cu-mediated conversion of substrate **A** into propargylic sulfone (*S*)-**B**. The energy values correspond to relative free energies at −30ºC and 1 M, and are provided in kcal/mol. The blue profile under (a) corresponds to the pathway leading to product (*R*)-**B**.

findings provide an unanticipated rationale for the observed enantio-induction that was experimentally observed (*vide infra*).

Relevance of the Proto-Demetalation Step. The occurrence of enantio-controlling proto-demetalation has thus far remained extremely rare in homogeneous catalysis. In 2017, Ackermann and coworkers reported an example related to Co-promoted C–H alkylation using DFT analysis,[12a,21] whereas in the following year Matsunaga et al. proposed the induction of enantioselectivity in the proto-demetalation step of a Rh-mediated C–H functionalization process.[12b] In line with these previous proposals, the two profiles shown in Figure 3 show that the key differentiation between the two pathways leading to (*S*) and (*R*) takes place when the protonated base (DIPEA-H$^+$) is in the coordination sphere of the Cu-complex. Thus, there is a vital role for the protonated base in the enantio-selection arising during the proto-demetalation step.

Origin of the Energy Difference at the TS4 Transition State. In order to explain why **TS4s** is more stable than **TS4r**, we performed an energy decomposition following a distortion/interaction model[22] as presented in Table 1. Full details of the computations are provided in the SI. Importantly, the potential energies reported in Table 1 do not exactly agree with the free energies listed in Figure 3, but nonetheless both predict the (*S*)-diastereoisomer of **TS4** as the most stable and are of a similar order of magnitude.

Out of the 5.4 kcal/mol of potential energy difference (with the (*S*)-diastereoisomer of **TS4** being more stable), 5.3 kcal/mol corresponds to the difference in distortion energy of the complex, meaning that the (*R*)-diastereoisomer undergoes a higher distortion when forming the complex-base adduct compared to the corresponding (*S*)-diastereoisomer. The difference in distortion of the base is negligible. Finally, out of the 5.4 kcal/mol, 0.1 kcal/mol come from interaction with the base with the (*R*)-diastereoisomer of the complex-base adduct having a slightly weaker interaction with the base than the (*S*)-diastereoisomer.

Table 1. Distortion/Interaction Analysis of the (*R*)- and (*S*)-Diastereoisomers of Transition States TS4[a]

		(*R*)	(*S*)	Δ(*R*–*S*)
E_1-E_o	base + complex	-8.6	-14.0	5.4
distortion	base	1.3	1.3	0.0
	complex	29.8	24.5	5.3
	total	31.1	25.8	5.3
interaction	base–complex	-39.7	-39.8	0.1

[a] The energies (all values in kcal/mol) presented are potential energies in vacuum. The sub-index '1' refers to the original geometries of **TS4s** and **TS4r**. The sub-index 'o' stands for the relaxed geometries of each fragment without the presence of the other fragment. Base stands here for DIPEA.

To rationalize what causes the differences in the distortion of the complex, we partitioned the transition state into two fragments, viz. the ligand-Cu being one of the fragments and the sulfone-DIPEA-H$^+$ as the second fragment. We looked into their non-covalent interactions using the reduced density gradient obtained using NCI PLOT 4.0 (Figure 4).[23] In both cases we can observe abundant interactions with the DIPEA-H$^+$, and both diastereoisomers feature π-π interactions between the phenyl groups of the sulfone and of the ligand. None of these interactions seem to cause the different stabilities of the TSs. However, a closer inspection at the bottom views of Figure 4 demonstrates that the (*S*)-diastereoisomer exhibits Cu–O interactions that are virtually non-existent in the (*R*)-diastereoisomer.

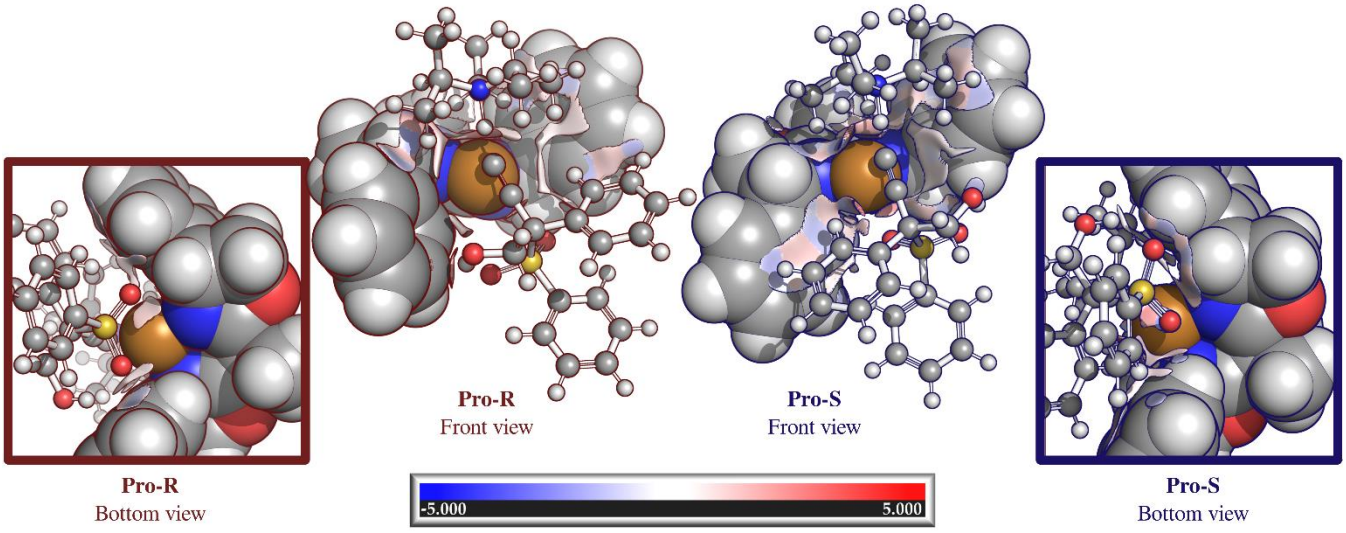

Figure 4. Reduced density gradient isosurfaces, value of 0.35, between the Cu-Ligand (van der Waals spheres) and the product-DIPEA-H$^+$ (ball and stick) obtained with NCI PLOTs for the **TS4r** (pro-*R*) and **TS4s** (pro-*S*). Isosurfaces are colored by the signed density, sign(λ_2)ρ. The blue regions match with strong favorable interactions whereas the red regions correspond to repulsive interactions.

Table 2. Comparison of Computationally and Experimentally Determined Enantiomeric Ratios in the Synthesis of Propargylic Sulfone B at –30 ºC[a]

		Computational			Exp.
Entry	Base	ΔΔG	*ee* (%)	S:R	S:R
1	DIPEA	2.5	98.9	99.5:0.5	96.5:3.5
2	TEA	0.3	28.4	64.2:35.8	95:5
3	DABCO	0.3	28.2	64.1:35.9	85:15
4	NMM	0.5	48.9	74.5:25.5	87:13

[a]All computed energies are in kcal/mol. TEA = triethyl amine, DABCO = 1,4-diazabicyclo[2.2.2]octane, NMM = *N*-methyl-morpholine.

The enantio-induction levels computed with other bases (using the ΔΔG values) in this propargylic sulfonylation reaction were calculated by DFT and compared against the previously attained experimental data (Table 2).[9] The agreement of the computed behavior of these other bases (TEA, DABCO and NMM) with experiment is not perfect, a result that is associated to the low energy differences involved. This may be related to different speciation of the catalytic intermediates involved while interacting with these potentially coordinating bases. Nevertheless, the trend that lower enantio-induction is attained compared to DIPEA under similar conditions is reproduced. These results suggest that the computational model used to describe the conversion of substrate **A** into propargylic sulfone **B** (Scheme 1b) is reasonable and allows to propose a key relationship between the base and the enantiomeric ratio.

CONCLUSIONS

With a combination of experimental and computational efforts, we have been able to achieve detailed insight into the mechanism of a previously reported Cu-promoted propargylic substitution reaction that leads to the formation of a sterically hindered carbon stereocenter. Contrary to previous paradigms in the asymmetric formation of elusive stereogenic centers, here we demonstrate that the enantiocontrol is exerted beyond the nucleophilic attack by the sulfonate anion (*i.e.*, C–S bond formation). A protodemetalation step is responsible for the enantio-discrimination of the process and we have been able to identify the crucial role that the base plays in this coupling manifold.

Additionally, we describe a detailed analysis of the preactivation pathway starting from a Cu(II) precursor, the following intermediates and the eventual formation of a catalytically competent Cu(I)Box complex. From the kinetic and DFT data, we conclude that a mono-nuclear Cu-derivative is involved in the productive catalytic cycle, and the previously observed NLE occurs at the Cu(I) oxidation state level with a heterochiral Cu(I)$(Box)_2$ as an off-cycle, inactive species. Our findings shed important light on a synthetically well-implemented C–heteroatom bond formation process empowered by a metal-mediated propargylic substitution, and offers novel mechanistic scenarios to forge tetrasubstituted tertiary and related quaternary carbon stereocenters.

ASSOCIATED CONTENT

Supporting Information

The Supporting Information is available free of charge at https://pubs.acs.org/doi/10.1021/jacs.###.

Experimental and analytical procedures, characterization of all new and relevant known compounds, computational details, additional free energy profiles and Cartesian coordinates of calculated structures (PDF)

Accession Codes

CCDC 2168195-2168201 contain the supplementary crystallographic data for this paper. These data can be obtained free of charge via www.ccdc.cam.ac.uk/data_request/cif, or by emailing data_request@ccdc.cam.ac.uk, or by contacting The Cambridge Crystallographic Data Centre, 12 Union Road, Cambridge CB2 1EZ, UK; fax: +44 1223 336033.

AUTHOR INFORMATION

Corresponding Authors

Arjan W. Kleij, *Institute of Chemical Research of Catalonia (ICIQ), The Barcelona Institute for Science & Technology (BIST), 43007 Tarragona, Spain; Catalan Institute of Research and Advanced Studies (ICREA), 08010 Barcelona, Spain;* orcid.org/0000-0002-7402-4764; Email: akleij@iciq.es

Feliu Maseras, *Institute of Chemical Research of Catalonia (ICIQ), The Barcelona Institute for Science & Technology (BIST), 43007 Tarragona, Spain;* orcid.org/0000-0001-8806-2019; Email: fmaseras@iciq.es

Authors

‡**Aleria Garcia-Roca** – *Institute of Chemical Research of Catalonia (ICIQ), The Barcelona Institute for Science & Technology (BIST), 43007 Tarragona, Spain;* orcid.org/0000-0003-4405-5372

‡**Raúl Pérez-Soto** – *Institute of Chemical Research of Catalonia (ICIQ), The Barcelona Institute for Science & Technology (BIST), 43007 Tarragona, Spain;* orcid.org/0000-0002-6237-2155

Georgiana Stoica – *Institute of Chemical Research of Catalonia (ICIQ), The Barcelona Institute for Science & Technology (BIST), 43007 Tarragona, Spain;* orcid.org/0000-0002-8599-3122

Jordi Benet-Buchholz – *Institute of Chemical Research of Catalonia (ICIQ), The Barcelona Institute for Science & Technology (BIST), 43007 Tarragona, Spain;* orcid.org/0000-0003-3984-3550

Notes

The authors declare no competing financial interest.

ACKNOWLEDGMENT

We thank the Cerca program/Generalitat de Catalunya, ICREA, MICINN (PID2020-112684GB-I00, PID2020-112825RB-I00, Severo Ochoa Excellence Accreditation 2020–2023 CEX2019-000925-S). R. P. S. thanks the Ministereo de Universidades for a predoctoral fellowship (FPU18/01138). We thank Dr. Bart Limburg for help regarding the analysis of the kinetic data.

REFERENCES

(1) For reviews see: (a) Roh, S. W.; Choi, K.; Lee, C. Transition Metal Vinylidene- and Allenylidene-Mediated Catalysis in Organic Synthesis. *Chem. Rev*. **2019**, *119*, 4293-4356. (b) Miyake, Y.; Uemura, S.; Nishibayashi, Y. Catalytic Propargylic Substitution Reactions. *ChemCatChem* **2009**, *1*, 342–356. (c) Detz, R. J.; Hiemstra, H.; van Maarseveen, J. H. Catalyzed Propargylic Substitution. *Eur. J. Org. Chem*. **2009**, 6263–6276. (d) Tsuji, H; Kawatsura, M. Transition-Metal-Catalyzed Propargylic Substitution of Propargylic Alcohol Derivatives Bearing an Internal Alkyne Group. *Asian J. Org. Chem*. **2020**, *9*, 1924–1941; (e) Roy, R.; Saha, S. Scope and Advances in the Catalytic Propargylic Substitution Reaction. *RSC Adv*. **2018**, *8*, 31129–31193.

(2) (a) Zhang D.-Y., Hu X.-P. Recent Advances in Copper-Catalyzed Propargylic Substitution. *Tetrahedron Lett*. **2015**, *56*, 283-295. (b) Nishibayashi, Y. Development of Asymmetric Propargylic Substitution Reactions Using Transition Metal Catalysts. *Chem. Lett*. **2021**, *50*, 1282-1288.

(3) Hattori, G.; Matsuzawa, H.; Miyake, Y.; Nishibayashi, Y. Copper-Catalyzed Asymmetric Propargylic Substitution Reactions of Propargylic Acetates with Amines. *Angew. Chem. Int. Ed*. **2008**, *47*, 3781–3783.

(4) Detz, R. J.; Delville, M. M. E.; Hiemstra, H.; van Maarseveen, J. H. Enantioselective Copper-Catalyzed Propargylic Amination. *Angew. Chem. Int. Ed.* **2008**, *47*, 3777–3780.

(5) (a) Li, R.-Z.; Liu, D.-Q.; Niu, D. Asymmetric O-Propargylation of Secondary Aliphatic Alcohols. *Nat. Catal*. **2020**, *3*, 672–680. (b) Nakajima, K.; Shibata, M.; Nishibayashi, Y. Copper-Catalyzed Enantioselective Propargylic Etherification of Propargylic Esters with Alcohols. *J. Am. Chem. Soc*. **2015**, *137*, 2472–2475. (c) Ikeda, M.; Miyake, Y.; Nishibayashi, Y. Cooperative Catalytic Reactions Using Distinct Transition-Metal Catalysts: Ruthenium- and Copper-Catalyzed Enantioselective Propargylic Alkylation. *Chem. Eur. J*. **2012**, *18*, 3321-3328. (d) Liu, S.; Tanabe, S.; Kuriyama, S.; Sakata, K.; Nishibayashi, S. Ruthenium- and Copper-Catalyzed Propargylic Substitution Reactions of Propargylic Alcohol Derivatives with Hydrazones. *Chem. Eur. J*. **2021**, *27*, 15650–15659. (e) Wang, B.; Liua, C.; Guo, H. Copper-Catalyzed Enantioselective Propargylic Substitution of Propargylic Acetates with Enamines. *RSC Adv*. **2014**, *4*, 53216-53219. (f) Li, Z.; Li, D.; Xiang, H.; Huang, J.; Zheng, Y.; Zhu, C.; Cui, X.; Chao, P.; Xu. H. Copper-Catalyzed Asymmetric Propargylic Substitution of Anthrones and Propargylic Esters. *Chin. Chem. Lett*. **2022**, *33*, 867-870. (g) Gao, X.; Xia, J.-L.; Zhang, S.; Wu, J.; Zhang, X. Copper-Catalyzed Enantioselective Trifluoromethylthiolation of Secondary Propargyl Sulfonates. *CCS Chem*. **2020**, *2*, 1463–147. (h) Tsuchida, K.; Yuki, M.; Nakajima, K.; Nishibayashi, Y. Copper- and Borinic Acid-catalyzed Propargylic Etherification of Propargylic Carbonates with Benzyl Alcohols. *Chem. Lett*. **2018**, *47*, 671-673.

(6) For examples related to the creation of quaternary carbon stereocenters under Cu-catalysis, see: (a) Tsuchida, K.; Senda, Y.; Nakajima, K.; Nishibayashi, Y. Construction of Chiral Tri- and Tetra-Arylmethanes Bearing Quaternary Carbon Centers: Copper-Catalyzed Enantioselective Propargylation of Indoles with Propargylic Esters. *Angew. Chem. Int. Ed*. **2016**, *55*, 9728–9732. (b) Li, H.; Grassi, D.; Guénée, L.; Bürgi, T.; Alexakis, A. Copper-Catalyzed Propargylic Substitution of Dichloro Substrates: Enantioselective Synthesis of Trisubstituted Allenes and Formation of Propargylic Quaternary Stereogenic Centers. *Chem. Eur. J*. **2014**, *20*, 16694–16706. (c) Han, F.-Z.; Zhu, F.-L.; Wang, Y.-H.; Zou, Y.; Hu, X.-H.; Chen, S.; Hu, X.-P. Highly Enantioselective Copper-Catalyzed Propargylic Substitution of Propargylic Acetates with 1,3-Dicarbonyl Compounds. *Org. Lett*. **2014**, *16*, 588–591. (d) Wen, Y.-H; Zhang, Z.-J.; Li, S.; Song, J.; Gong, L.-Z. Stereodivergent Propargylic Alkylation of Enals via Cooperative NHC and Copper Catalysis. *Nat. Commun*. **2022**, *13*, 1344.

(7) For illustrative examples: (a) Cai, A.; Guo, W.; Martínez-Rodríguez, L.; Kleij, A. W. Palladium-Catalyzed Regio- and Enantio-Selective Synthesis of Allylic Amines Featuring Tetrasubstituted Tertiary Carbons. *J. Am. Chem. Soc*. **2016**, *138*, 14194-14197. (b) Guo, W.; Cai, A.; Xie, J.; Kleij, A. W. Asymmetric Synthesis of alfa,alfa-Disubstituted Allylic Amines via Pd-Catalyzed Allylic Substitution. *Angew. Chem. Int. Ed.* **2017**, *56*, 11797-11801. (c) Cai, A.; Kleij, A. W. Regio- and Enantioselective Preparation of Chiral Allylic Sulfones Featuring Elusive Quaternary Stereocenters. *Angew. Chem. Int. Ed.* **2019**, *58*, 14944-14949. (d) Gómez, J. E.; Guo, W.; Gaspa, S.; Kleij, A. W. Copper-Catalyzed Synthesis of gamma-Amino Acids Featuring Quaternary Stereocenters. *Angew. Chem. Int. Ed*. **2017**, *56*, 15035-15038.

(8) (a) Quasdorf, K. W.; Overman, L. E. Catalytic Enantioselective Synthesis of Quaternary Carbon Stereocentres. *Nature* **2014**, *516*, 181-191. (b) Li, C.; Ragab, S. S.; Liu, G.; Tang, W. Enantioselective Formation of Quaternary Carbon Stereocenters in Natural Product Synthesis: a Recent Update. *Nat. Prod. Rep*. **2020**, 37, 276-292. (c) Feng, J.; Holmes, M.; Krische, M. J. Acyclic Quaternary Carbon Stereocenters via Enantioselective Transition Metal Catalysis. *Chem. Rev*. **2017**, *117*, 12564–12580.

(9) Gómez, J. E.; Cristòfol, À.; Kleij, A. W. Copper-Catalyzed Enantioselective Construction of Tertiary Propargylic Sulfones. *Angew. Chem. Int. Ed.* **2019**, 58, 3903-3907.

(10) (a) Hattori, G.; Sakata, K.; Matsuzawa, H.; Tanabe, Y.; Miyake, Y.; Nishibayashi, Y. Copper-Catalyzed Enantioselective Propargylic Amination of Propargylic Esters with Amines: Copper–Allenylidene Complexes as Key Intermediates. *J. Am. Chem. Soc*. **2010**, *132*, 10592–10608. For studies related to other metal(allenylidene)s, see: (b) Nishibayashi, Y.; Wakiji, I.; Hidai, M. Novel Propargylic Substitution Reactions Catalyzed by Thiolate-Bridged Diruthenium Complexes via Allenylidene Intermediates. *J. Am. Chem. Soc*. **2000**, *122*, 11019-11020. (c) Liu, S.; Tanabe, Y.; Kuriyama, S.; Sakata, K.; Nishibayashi, Y. Ruthenium-Catalyzed Enantioselective Propargylic Phosphinylation of Propargylic Alcohols with Phosphine Oxides. *Angew. Chem. Int. Ed*. **2021**, *60*, 11231-11236. For a review on this topic, see: (d) Sakata, K.; Nishibayashi, Y. Mechanism and Reactivity of Catalytic Propargylic Substitution Reactions via Metal–Allenylidene Intermediates: a Theoretical Perspective. *Catal. Sci. Technol*. **2018**, *8*, 12–25.

(11) Armstrong, B. M.; Sayler, R. I.; Shupe, B. H.; Stich, T. A.; Britt, R. D.; Franz, A. K. EPR Evidence for the Origin of Nonlinear Effects in an Enantioselective Cu(II)-Catalyzed Spiroannulation. *ACS Catal*. **2019**, *9*, 1224–1230.

(12) Enantiocontrol exerted at the stage of protodemetalation is rare, see: (a) Pesciaioli, F.; Dhawa, U.; Oliveira, J. C. A.; Yin, R.; John, M.; Ackermann, L. Enantioselective Cobalt(III)-Catalyzed C–H Activation Enabled by Chiral Carboxylic Acid Cooperation. *Angew. Chem. Int. Ed*. **2018**, *57*, 15425–15429. (b) Satake, S.; Kurihara, T.; Nishikawa, K.; Mochizuki, T.; Hatano, M.; Ishihara, K.; Yoshino, T.; Matsunaga, S. Pentamethylcyclopentadienyl Rhodium(III)–Chiral Disulfonate Hybrid Catalysis for Enantioselective C–H Bond Functionalization. *Nat. Catal*. **2018**, *1*, 585–591.

(13) (a) Burés, J. Variable Time Normalization Analysis: General Graphical Elucidation of Reaction Orders from Concentration Profiles. *Angew. Chem. Int. Ed.* **2016**, *55*, 16084-16087. (b) Nielsen,

C. D.-T.; Burés, J. Visual Kinetic Analysis. *Chem. Sci*. **2019**, *10*, 348-353.

(14) Note that Evans and coworkers reported on the use of Cu(Box) complexes in Lewis acid mediated enantioselective catalysis, including complex **1** and its X-ray structure, see: (a) Evans, D. A.; Burgey, C. S.; Paras, N. A.; Vojkovsky, T.; Tregay, S. W. C2-Symmetric Copper(II) Complexes as Chiral Lewis Acids. Enantioselective Catalysis of the Glyoxylate–Ene Reaction. *J. Am. Chem. Soc.* **1998**, 120, 5824-5825. (b) Evans, D. A.; Tregay, S. W.; Burgey, C. S.; Paras, N. A.; Vojkovsky, T. C2-Symmetric Copper(II) Complexes as Chiral Lewis Acids. Catalytic Enantioselective Carbonyl–Ene Reactions with Glyoxylate and Pyruvate Esters. *J. Am. Chem. Soc*. **2000**, *122*, 7936–7943. (c) Feng, F.-F.; Wang, X.-Q.; Sun, L.; Cheung, C. W.; Nie, J.; Ma, J.-U. Switching of Enantioselectivity in the Cu-Catalyzed Asymmetric Decarboxylative Aldol Reaction of Tryptanthrin with β-Keto Acids: An Unexpected Counteranion Effect. *Org. Lett*. **2021**, *23*, 4379-4384.

(15) Both Franz and Murphy independently reported the EPR analysis of homochiral complex **2**, see: Owen, M. E.; Carter, E.; Hutchings, G. J.; Ward, B. D.; Murphy, D. M. Influence of Counterions on the Structure of Bis(Oxazoline)Copper(II) Complexes; an EPR and ENDOR Investigation. *Dalton Trans.* **2012**, *41*, 11085-11092 and ref. 11.

(16) Limited examples of Cu(I) complexes with a T-shaped coordination geometry: (a) van der Vlugt, J. I.; Pidko, E. A.; Vogt, D.; Lutz, M.; Spek, A. L.; Meetsma, A. T-Shaped Cationic Cu^{I} Complexes with Hemilabile PNP-Type Ligands. *Inorg. Chem*. **2008**, *47*, 4442–4444. (b) Tano, T.; Mieda, K.; Sugimoto, H.; Ogra, T.; Itoh, S. A Copper Complex Supported by an N_2S-Tridentate Ligand Inducing Efficient Heterolytic O–O Bond Cleavage of Alkylhydroperoxide. *Dalton Trans*. **2014**, *43*, 4871–4877; (c) Bezuidenhout, D. I.; Kleinhans, G.; Guisado-Barrios, G.; Liles, D. C.; Ung, G.; Bertrand, G. Isolation of a Potassium Bis(1,2,3-Triazol-5-Ylidene)Carbazolide: a Stabilizing Pincer Ligand for Reactive Late Transition Metal Complexes. *Chem. Commun*. **2014**, *50*, 2431–2433. (d) Kleinhans, G.; Chan, A. K.-W.; Leung, M.-Y.; Liles, D. C.; Fernandes, M. A.; Yam, V. W.-W.; Fernández, I.; Bezuidenhout, D. I. Synthesis and Photophysical Properties of T-Shaped Coinage-Metal Complexes. *Chem. Eur. J*. **2020**, *26*, 6993–6998.

(17) When Cu(II) complex **2** was treated in similar way with the same reagent combination though in the presence of O_2, no formation of the target Cu(I)acetylide or complex **5** could be observed as evidenced by EPR studies. See the SI for details.

(18) (a) Girard, C.; Kagan, H. B. Nonlinear Effects in Asymmetric Synthesis and Stereoselective Reactions: Ten Years of Investigation. *Angew. Chem. Int. Ed*. **1998**, *37*, 2922–2959. (b) Satyanarayana, T.; Abraham, S.; Kagan, H. B. Nonlinear Effects in Asymmetric Catalysis. *Angew. Chem. Int. Ed*. **2009**, *48*, 456–494.

(19) (a) Calculations used the B3LYP-D3 functional and included optimizations in solvent. Full computational details are given in the SI. (b) A data set of all computational results is available in the ioChem-BD repository at https://iochem-bd.iciq.es/browse/review-collection/100/39998/7849f53e5126c66aa6df6082. (c) See for general reference: Álvarez-Moreno, M.; de Graaf, C.; López, N.; Maseras, F.; Poblet, J. M.; Bo, C. Managing the Computational Chemistry Big Data Problem: The ioChem-BD Platform. *J Chem. Inf. Model.* **2015**, 55, 95-103.

(20) The *Si*-attack leads to (*S*)-**B** sulfone product whereas *Re*-attack provides (*R*)-B.

(21) Zell, D.; Bursch, M.; Müller, V.; Grimme, S.; Ackermann, L. Full Selectivity Control in Cobalt(III)-Catalyzed C-H Alkylations by Switching of the C-H Activation Mechanism. *Angew. Chem. Int. Ed*. **2017**, *56*, 10378-10382.

(22) Bickelhaupt, F. M.; Houk, K. N. Analyzing Reaction Rates with the Distortion/Interaction-Activation Strain Model. *Angew. Chem. Int. Ed*. **2017**, *56*, 10070-10086.

(23) (a) Contreras-Garcia, J.; Johnson, E. R.; Keinan, S.; Chaudret, R.; Piquemal, J-P.; Beratan, D. N.; Yang, W. NCIPLOT: A Program for Plotting Noncovalent Interaction Regions. *J. Chem. Theory Comput.* **2011**, *7*, 625-632. (b) Johnson, E. R.; Keinan, S.; Mori-Sanchez, P.; Contreras-Garcia, J; Cohen, A. J.; Yang, W. Revealing Noncovalent Interactions. *J. Am. Chem. Soc*. **2010**, *132*, 6498-6506. (c) Boto, R. A.; Peccati, F.; Laplaza, R.; Quan, C.; Carbone, A.; Piquemal, J.-P.; Maday, Y.; Contreras-Garcia, J. NCIPLOT4: Fast, Robust, and Quantitative Analysis of Noncovalent Interactions. *J. Chem. Theory Comput*. **2020**, *16*, 7-17.

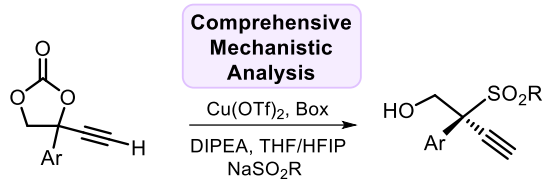

- *Proto-demetalation drives asymmetric induction*
- *NLE observed at the Cu(I) oxidation state*
- *Crucial role for the base additive*
- *Isolation/characterization of key intermediates*

(Table of Contents Entry)